PCCP

RSC Publishing

PAPER

View Article Online
View Journal | View Issue

Cite this: *Phys. Chem. Chem. Phys.*, 2013, **15**, 11468

The interplay of hydrogen bonding and dispersion in phenol dimer and trimer: structures from broadband rotational spectroscopy†

Nathan A. Seifert,[a] Amanda L. Steber,[a] Justin L. Neill,[a] Cristóbal Pérez,[a] Daniel P. Zaleski,[a] Brooks H. Pate*[a] and Alberto Lesarri*[b]

Received 22nd April 2013,
Accepted 31st May 2013

DOI: 10.1039/c3cp51725j

www.rsc.org/pccp

The structures of the phenol dimer and phenol trimer complexes in the gas phase have been determined using chirped-pulse Fourier transform microwave spectroscopy in the 2–8 GHz band. All fourteen ^{13}C and ^{18}O phenol dimer isotopologues were assigned in natural abundance. A full heavy atom experimental substitution structure was determined, and a least-squares fit ground state r_0 structure was determined by proper constraint of the M06-2X/6-311++g(d,p) *ab initio* structure. The structure of phenol dimer features a water dimer-like hydrogen bond, as well as a cooperative contribution from inter-ring dispersion. Comparisons between the experimental structure and previously determined experimental structures, as well as *ab initio* structures from various levels of theory, are discussed. For phenol trimer, a C_3 symmetric barrel-like structure is found, and an experimental substitution structure was determined *via* measurement of the six unique ^{13}C isotopologues. The least-squares fit $r_m^{(1)}$ structure reveals a similar interplay between hydrogen bonding and dispersion in the trimer, with water trimer-like hydrogen bonding and C–H$\cdots\pi$ interactions.

Introduction

The structure of the phenol dimer presents a challenge to computational chemistry because the hydrogen bond interaction of the hydroxyl group and the dispersion interaction of the benzene ring prefer different geometries.[1–3] Since dispersion is ignored in the Hartree–Fock approximation[4] and traditional DFT functionals treat it incompletely, accurate predictions are immediately limited to post-Hartree–Fock methods such as MP2 or coupled cluster, or dispersion-modified density functional theory.[5–9] However, results for phenol dimer using these advanced levels of theory give inconsistent results in the treatment of dispersion.[3] It is therefore important for an accurate experimental structure to be determined in order to not only accurately gauge the efficacy of these methods,[10–11] but also to provide an experimental perspective on an interplay of competing non-covalent interactions that play an essential role in everything from biochemical processes[12,13] to catalysis[14,15] and supramolecular chemistry.[16]

This intriguing interplay of non-covalent interactions in phenol dimer has not gone unnoticed, as a number of theoretical and spectroscopic studies have been published over the past few decades, beginning with the multiphoton ionization studies of Fuke and Kaya.[17,18] Phenol dimer is a member of the JSCH-2005 benchmark, which was created for the purpose of benchmarking the efficacy of new and existing theoretical methods in treating noncovalent interactions in biologically-relevant systems.[19] Experimental structural studies have also been previously published and performed with a variety of spectroscopic methods including rotational coherence spectroscopy (RCS),[20,21] IR-UV double resonance spectroscopy,[22,23] and high-resolution UV absorption spectroscopy.[24] The RCS measurements have provided rotational constants for the phenol dimer and important features of the molecular structure with comparison to *ab initio* predictions have also been discussed.[1] Subsequent high-resolution UV spectroscopy studies determined the molecular rotational constants to higher precision.[25] Also, the spectra of several, commercially available isotopic species were analyzed to provide more detail about the structure of phenol dimer.[24]

Although these methods have shed considerable light on the structure of phenol dimer, they lack the high resolution and

[a] *Department of Chemistry, University of Virginia, McCormick Road, Charlottesville, Virginia 22904, USA. E-mail: brookspate@virginia.edu*
[b] *Departamento de Química Física y Química Inorgánica, Facultad de Ciencias, Universidad de Valladolid, 47011 Valladolid, Spain. E-mail: lesarri@qf.uva.es*

† Electronic supplementary information (ESI) available. See DOI: 10.1039/c3cp51725j

structural precision afforded by high resolution microwave spectroscopy. In this study, the use of chirped-pulse Fourier transform microwave (CP-FTMW) spectroscopy[26] in the 2–8 GHz band[27] enables the determination of a full heavy atom (*e.g.* carbons and oxygens) experimental structure of phenol dimer, which is in excellent agreement with *ab initio* results. This structure, as well as the least-squares fitted, ground state r_0 structure determined in this study, resolves a number of the inconsistencies between previous experimental structures[21,24] of phenol dimer and the *ab initio* results, including the hydrogen bonding distance and the relative orientations of the two benzene rings due to dispersive interactions. It should be noted that we have previously published a study on phenol dimer, including the heavy atom substitution structure, using reduced bandwidth measurements in the 6.5–18 GHz range.[28] However, that study was limited in scope compared to the results presented here, and the data collected and analyzed for this study is completely independent of the data used in the previous microwave study.

In addition, we report the first direct structural determination of phenol trimer, which has a symmetric, barrel-like structure. Although the trimer was previously detected and correctly assigned to a barrel structure in the aforementioned IR-UV double resonance study,[22] no direct structural information could be obtained from the O–H stretch region vibrational band data. Like phenol dimer, the trimer features an interplay between dispersion and hydrogen bonding. The trimer suffers some of the inconsistencies between varying levels of theory like the dimer, though the constraint of C_3 symmetry reduces the number of independent degrees of freedom, so potential differences between the observed and calculated structure that can reduce the quality of the spectroscopic predictions are less prevalent than in the dimer. However, the correct choice of theory produces a good trimer prediction, and the theoretical results reported here are in good agreement with experimental results.

Experimental

The broadband rotational spectrum of the phenol clusters was measured in the 2–8 GHz frequency range using a CP-FTMW spectrometer. The spectrometer has two upgrades from the previous design. A new set of high-gain microwave horn antennas (Q-Par Angus WBH 2-18-NHG) are used to broadcast the high-power chirped-pulse and receive the broadband molecular emission. The higher directionality of these horns makes it possible to increase the horn separation to 140 cm and, therefore, to include five pulsed nozzle sources. As has been discussed previously, the use of a 5-nozzle sample injection system in CP-FTMW spectrometers reduces the measurement time required to reach a target sensitivity by 25 and reduces the sample consumption by a factor of 5 over a single pulsed nozzle system. The new antenna set yields markedly better performance in the 2–4 GHz region over the previous spectrometer and improved sensitivity at low frequency is important for the study of large clusters like the phenol trimer. The spectrometer uses a new pulsed traveling wave tube amplifier (Applied Systems Engineering 167S/C) that gives higher peak power (600 W) than was used in the previous CP-FTMW spectrometer design.

Phenol is loaded into the reservoir of the pulsed nozzles and heated to 85 °C. Neon carrier gas at a pressure of 1.67 atm is used for the pulsed jet expansion with a pulse duration of 700 μs. We estimate that each nozzle pulse consumes 10 nmol of phenol. Following gas sample injection into the spectrometer vacuum chamber, a series of 8 back-to-back measurements of the broadband rotational spectrum are performed. These measurements use a 4 μs duration chirped-pulse with a linear frequency sweep from 2–8 GHz. The chirped-pulse is generated by a 24 Gs s^{-1} arbitrary waveform generator (Tektronix AWG 7122B) and sent directly to the traveling wave tube amplifier. Following sample excitation, the coherent broadband emission, of free induction decay, is amplified in a high-gain, low-noise microwave amplifier and digitized using an 8-bit, 25 Gs s^{-1} digitizer of a digital oscilloscope (Tektronix DPO73304D). The FID is collected for 40 μs. The data processing methods used in the digital oscilloscope are optimized for signal averaging CP-FTMW data. The 8 spectra acquired for each gas sample injection are first averaged into a single record in the high-speed memory of the digitizer and this data is then moved into standard memory for subsequent time-domain signal averaging. This new data analysis algorithm has produced a factor of 9 increase in the measurement rate for the CP-FTMW spectrometer. Gas sample injection repetition rates of 8 Hz (64 Hz FID signal averaging) are achieved. The 2–8 GHz spectrum of phenol used in this analysis contained a total of 9.2 M FID averages. The frequency domain spectrum is obtained from this averaged FID by fast Fourier transformation following the application of a Kaiser–Bessel window function to give improved baseline resolution in the spectrum. The lists of assigned transitions are provided in the ESI.†

Results

A section of the 2–8 GHz broadband rotational spectrum of the pulsed-jet phenol sample is shown in Fig. 1. This figure also shows the importance in applying the Kaiser–Bessel window function to improve the baseline resolution so that weak transitions, from natural abundance isotopic species for example, can be detected in the presence of the strong phenol and phenol dimer rotational transitions. The ability to shape the rotational spectrum line shape is a special feature of broadband rotational spectroscopy. In comparison, the narrow bandwidth of a cavity-FTMW spectrometer results in the polarization of molecules "in the wings" of the inhomogeneous residual Doppler distribution making it impossible to minimize the baseline resolution of very strong transitions.[29] Although CP-FTMW spectrometers have lower resolution when defined as the full-width at half-maximum, their superior baseline resolution yields a higher useable dynamic range in the measurement.

The strongest transitions in the spectrum come from the phenol monomer and have about 30 000 : 1 signal-to-noise ratio. The spectrum for the phenol dimer is a factor of 10 weaker. The measurement sensitivity, therefore, is sufficient to observe the singly ^{13}C and ^{18}O isotopologues of the phenol dimer in natural abundance. The full 2–8 GHz spectrum, as well as an expanded region showing the ^{13}C isotopic spectra in natural abundance,

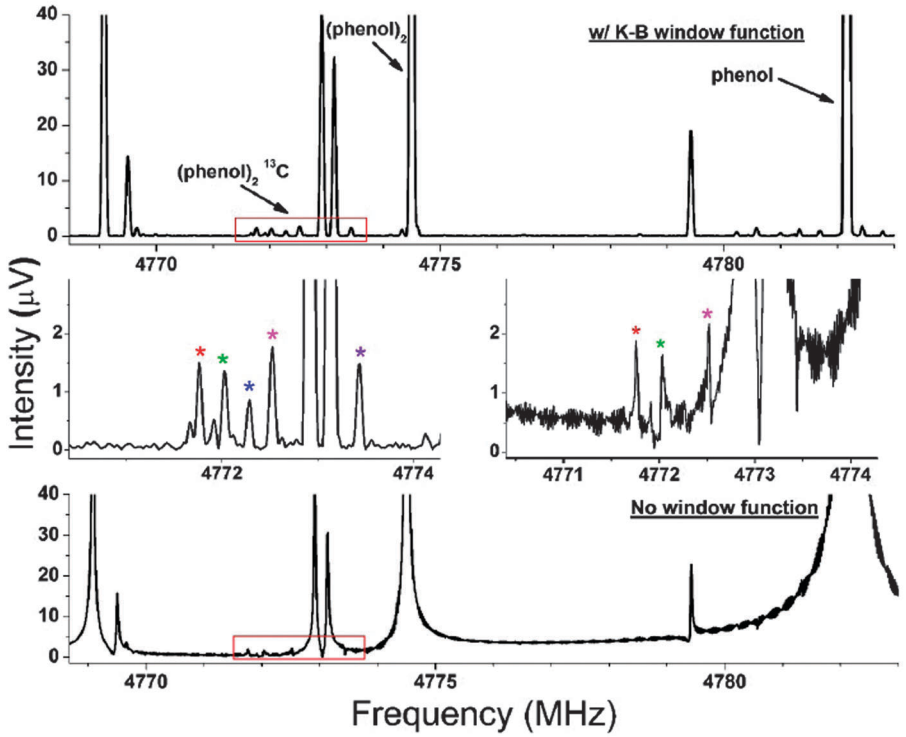

Fig. 1 A 20 MHz section of the 2–8 GHz CP-FTMW spectrum of phenol. Use of the Kaiser–Bessel window function (top spectrum) greatly improves the baseline resolution, enabling observation of multiple transitions of the ^{13}C isotopologues of phenol dimer (starred, center) that are poorly resolved or not resolved at all in the raw spectrum (bottom).

is shown in Fig. 2. A summary of the rotational spectrum analysis of the phenol dimer and the 14 heavy-atom isotopologues using the A-reduction of the Watson Hamiltonian[30] is presented in Table 1. The centrifugal distortion constants for the isotopologues were fixed to the normal isotopic species fit values (fitting these constants for each isotopologues produced nearly the same values within the confidence interval of the parameter estimation).

The phenol trimer is observed in the spectrum as an oblate symmetric top species, as seen in Fig. 3. With the improved spectrometer performance, we have been able to observe the ^{13}C isotopologues of phenol trimer in natural abundance ($\sim$1% abundance). Since the phenol trimer is C_3 symmetric, the intensities of the isotopologues were tripled due to symmetry. For ease of analysis, the prolate I^r representation was chosen for assignment of the isotopologues. Since the isotopic substitutions are off the C_3 symmetry axis, isotopologues of phenol trimer in the prolate basis show pure μ_c-type asymmetric top spectra. However, since the asymmetry generated by a single ^{13}C substitution is slight, isotopologues with substitutions near the symmetry axis generate small asymmetry splittings. Since assignments for these isotopologues include transitions with a relatively high J quantum number ($J \leq 14$), the region where transitions with a high K_c appear for a given J tend to be quite dense. Since these high K_c transitions are essential in determining the distortion for a given species, floating distortion was only possible for the *para*-substituted and a *meta*-substituted isotopologue, where the asymmetry is relatively high. A visual summary of the phenol trimer spectrum can be seen in Fig. 4.

We have identified two other symmetric top species in the spectrum with rotational constants similar to the normal species of phenol trimer. These spectra are about 30 times weaker than the normal species phenol trimer. Because we cannot propose a plausible phenol trimer isomer that is a symmetric top with nearly the same rotational constant of the dominant species, we believe that these spectra come from vibrationally excited states of the assigned trimer species that are populated in the pulsed molecular beam. The harmonic vibrational calculation at the M06-2X/6-311++g(d,p) level of theory,[31,32] gives 6 vibrational normal modes with frequencies below 100 cm^{-1}. The computed vibrational frequencies are provided in the ESI.† A summary of the spectral analysis of all phenol trimer species in provided in Table 2. All calculations done for this study were performed exclusively with the GAUSSIAN 09, Rev A.02 suite of programs.[33]

Discussion

The analysis of the rotational spectra of the isotopologues can be used to generate experimental structures of the phenol dimer and trimer. The rotational constants for each isotopologue can be converted into the position of the substituted atom in the principal axis system using the method first described by Kraitchman[34] and analyzed by Costain.[35] This method builds the experimental structure atom-by-atom and requires no direct

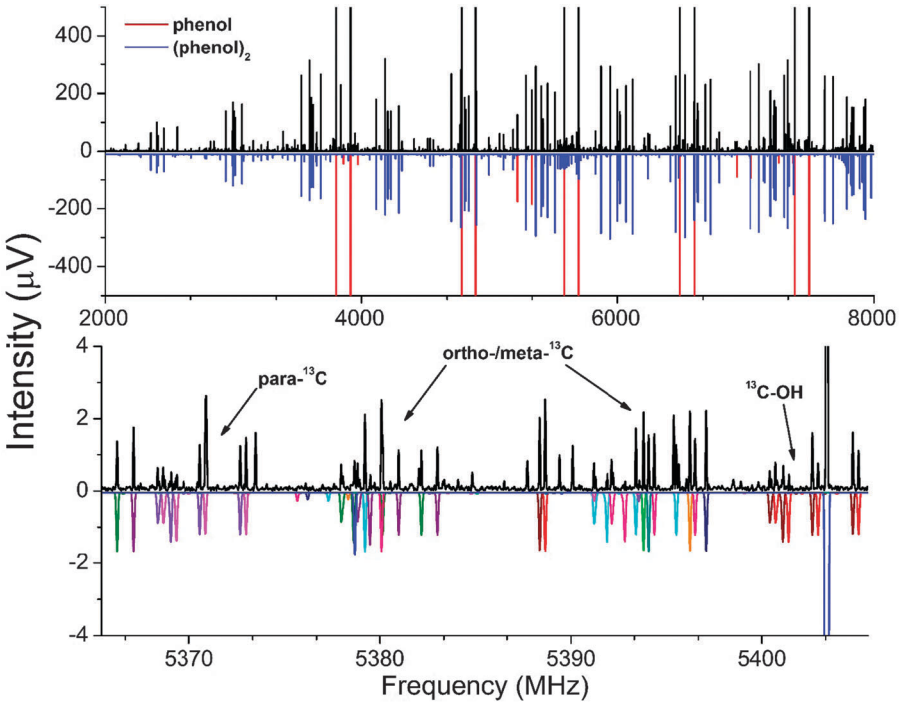

Fig. 2 The 2–8 GHz spectrum of phenol, with 2 K predictions of phenol monomer (top, red) and phenol dimer (top, blue). The full dynamic range of the phenol monomer transitions has been truncated in order to emphasize the phenol dimer spectrum. The ^{13}C isotopologues of phenol dimer (bottom) are also compared to predictions (bottom, multiple colors). As shown, the isotopologues can be seen as spatially resolved in frequency space, where the substitutions farthest from the center of mass are the most redshifted from the parent transition (bottom, strong blue transition at *ca.* 5403 MHz). ^{18}O isotopologues are not shown.

Table 1 Spectroscopic parameters for phenol dimer and its 14 heavy atom isotopologues. *N* is the total number of transitions contained in the fit, and σ is the RMS average of each fit. Distortion for all isotopologues is held fixed to the reported parent species values

	Parent	Donor	*A* (MHz)	*B*	*C*	*N*	σ (kHz)
A (MHz)	1415.32747(14)	1-^{13}C	1413.0983(14)	312.52409(32)	287.16539(32)	120	8.08
B	313.368020(41)	2-^{13}C	1412.74240(48)	312.75594(19)	287.52814(20)	136	5.77
C	287.961282(38)	3-^{13}C	1403.8469(63)	312.00616(35)	286.73261(34)	111	8.25
		4-^{13}C	1406.0358(10)	310.68675(28)	285.40748(28)	129	7.98
Δ_J (kHz)	0.372930(76)	5-^{13}C	1413.37840(97)	310.05088(26)	285.13627(28)	133	8.75
Δ_{JK}	−3.92349(48)	6-^{13}C	1411.85779(88)	311.08467(29)	286.08891(29)	113	6.98
Δ_K	13.0664(27)	1-^{18}O	1387.525(25)	312.54360(80)	286.32269(76)	60	10.4
δ_J	0.057377(17)	Acceptor					
δ_K	0.6928(19)	1-^{13}C	1413.23440(69)	312.50304(16)	287.15363(16)	123	5.53
		2-^{13}C	1412.24751(35)	312.72811(22)	287.52476(22)	133	5.38
N	481	3-^{13}C	1403.92180(82)	311.90897(22)	286.72685(23)	129	7.11
σ (kHz)	6.39	4-^{13}C	1405.66540(96)	310.71737(19)	285.40780(19)	123	6.79
		5-^{13}C	1413.02009(74)	310.10090(26)	285.17718(26)	121	6.41
		6-^{13}C	1411.56899(64)	311.12121(17)	286.14677(18)	136	6.84
		2-^{18}O	1388.945(42)	312.70639(67)	286.47370(65)	69	7.02

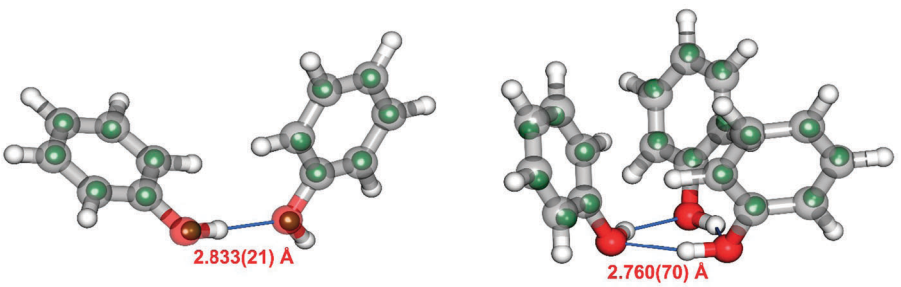

Fig. 3 Structures of the phenol dimer and trimer. In both cases, the shown frameworks are the r_0 and $r_m^{(1)}$ structures for phenol dimer and trimer respectively, derived from M06-2X/6-311++g(d,p) geometries and experimental data. The green inner spheres represent the Kraitchman coordinates derived directly from the experimental data. The labeled O···O lengths are taken from the r_0 and $r_m^{(1)}$ geometries.

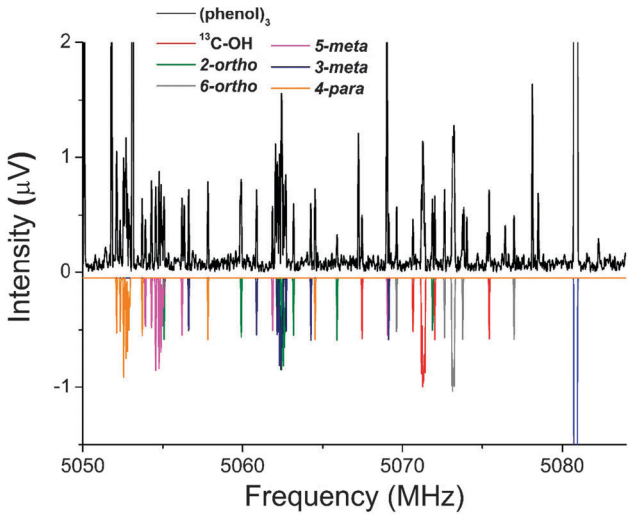

Fig. 4 A section of the 2–8 GHz spectrum representing the $J = 9–8$ transition of phenol trimer (top), with 2 K predictions of the parent species and the 6 ^{13}C isotopologues (bottom). As seen, the asymmetry generated by the ^{13}C substitution is slight, and leads to dense pile-ups of high K_c, μ_c-type transitions.

input from theoretical calculations. However, the analysis provides only the magnitudes of the principal axis coordinates. In this work, there are theoretical structures available that have calculated rotational constants that are in good agreement with experiment and, therefore, are likely to be good approximations of the experimental structures. We have used these theoretical structures to guide the selection of the signs of the coordinates for each atom in the ''substitution structure.'' Once a close match between the experimental and theoretical heavy-atom structure is obtained, it is possible to produce a ''refined'' structure that fits structural parameters directly to the observed isotopic moments-of-inertia using a limited set of constraints from the theoretical model.

The structure of the phenol dimer

The experimental heavy atom substitution structure of the phenol dimer, showing the positions of the twelve distinct carbon atoms and the two oxygen atoms, is shown in Fig. 3. The experimental atom positions in the principal axis system are available in the ESI.† The phenol dimer structure is nearly symmetric (only the free O–H reduces the symmetry) and the carbon atoms appear in pairs with nearly identical atom magnitudes of the coordinate positions. In this case, there is the possibility that atom pairs have not been properly assigned. However, the effect of changing the positions has negligible effect on the experimental substitution structure. The phenyl ring structure from this analysis shows small deviations from planarity. In a few cases of structure determination of rigid, aromatic molecules by rotational spectroscopy we have observed more planar structures. It is likely that the effects of large amplitude vibrational motions are responsible for the deviations from planarity observed for phenol dimer.

A key structural parameter for the phenol dimer is the ''hinge'' angle between the two phenol rings. This aspect of the geometry reflects the balance between the intermolecular hydrogen bond and the dispersion interaction of the aromatic rings. The experimental values for the hinge angle form the current work, a previous rotationally-resolved UV spectroscopic study,[24] and several computational chemistry models are given in Table 3. As discussed before, different computational models predict significantly different equilibrium geometries for the phenol dimer.[3] In particular, the incomplete treatment of dispersion in density functional theory leads to a structure with a large hinge angle that is dominated by the geometry preference of the hydrogen bond. Functionals with exchange–correlation energy approximations that have improved treatment of dispersion interactions, like M06-2X, give equilibrium structures that better match the experimental structure. The equilibrium structures from MP2/6-311++g(d,p) also give good approximations to the geometry that we have observed in experiment. However, as the basis set size increases, the MP2 theoretical geometries give angles that are smaller than experiment suggesting that the stabilization energy due to dispersion is overestimated.[36] Similar problems are seen in the CCSD calculations with Pople basis sets, though in this case CCSD actually underestimates the dispersion, with larger hinge angles than experiment. Hybrid functionals like M06-2X give results that appear to stabilize as one increases basis set size. This is consistent with previous theoretical results, where high level dispersion modified DFT calculations, such as the RI-DFT-D/aQZ′ results by Kolář and Hobza, give excellent results compared to experiment.[3] A visual comparison of three different levels of theory with experiment can be found in Fig. 5.

One important assumption behind the comparisons between the substitution structure and theoretical equilibrium

Table 2 Spectroscopic parameters for phenol trimer and its 6 ^{13}C isotopologues. Distortion was fit for the most abundant species, as well as for ^{13}C isotopologues 4 and 6. Distortion parameters for the other ^{13}C isotopologues were fixed to the average of isotopologues 4 and 6

	Parent	1-^{13}C	6-^{13}C	2-^{13}C	5-^{13}C	3-^{13}C	4-^{13}C
A (MHz)	—	282.19749(14)	282.21553(17)	282.26789(23)	282.23405(52)	281.96181(31)	281.89683(66)
B (MHz)	282.280790(56)	281.30995(14)	280.33503(17)	281.44815(23)	279.47608(53)	280.56222(30)	279.57290(65)
C (MHz)	—	187.33(14)	187.069(50)	187.36(21)	186.897(44)	187.34(14)	186.824(66)
Δ_J (kHz)	0.10300(19)	[0.0315]	[0.0315]	[0.0315]	0.0297(10)	[0.0315]	0.0334(12)
Δ_{JK}	−0.13600(28)	[0.0752]	[0.0752]	[0.0752]	0.0779(26)	[0.0752]	0.725(34)
Δ_K	—	[0]	[0]	[0]	[0]	[0]	[0]
δ_J	—	[0.03249]	[0.03249]	[0.03249]	0.03227(56)	[0.03249]	0.03270(65)
δ_K	—	[0]	[0]	[0]	[0]	[0]	[0]
N	20	63	87	53	108	53	100
σ (kHz)	1.37	5.96	7.11	9.10	9.33	9.49	8.62

Table 3 Phenol dimer rotational constants and hinge angles from various levels of theory

	A (MHz)	*B* (MHz)	*C* (MHz)	Hinge angle
MP2/6-311g(d,p)	1165.2	410.3	363.3	49.0
MP2/6-311++g(d,p)	1365.2	325.8	305.7	69.5
MP2/cc-PVTZ-cp[a]	1286.0	356.1	317.6	64.4
CCSD/6-311g(d,p)	1545.2	282.4	275.6	88.7
CCSD/6-311++g(d,p)	1459.6	308.9	286.8	79.5
M06-2X/6-311g(d,p)	1352.7	342.1	318.3	68.2
M06-2X/6-311++g(d,p)	1382.5	336.6	306.4	59.6
M06-2X/6-311++g(df,pd)	1382.9	338.4	307.6	59.6
B3LYP/6-31G(d,p)	1800.0	250.8	243.7	111.9
B3LYP/6-311++g(d,p)	1946.3	231.8	229.6	110.5
RI-DFT-D/aQZ′[b]	1399.7	318.5	292.5	61
CP-FTMW (r_0, this study)	1415.3275(11)	313.36802(32)	287.96128(30)	62.3(14)
UV-VIS (r_0, Schmitt *et al.*)	1416.99(39)	313.51(1)	288.11(1)	63.0

[a] Taken from ref. 19. [b] Taken from ref. 3.

geometries is that the hinge angle is well-defined in the dimer. The ''hinge motion'' of the dimer correlates to the lowest frequency normal-mode vibration with a harmonic frequency of 28 cm^{-1} calculated at the M06-2X/6-311++g(d,p) level. This is high compared to the measured frequency[37] of 9 cm^{-1} but other calculations obtain similar results, though it appears the application of counterpoise correction enables a more accurate estimation of this mode's vibrational energy.[25] We have estimated the one-dimensional potential energy of this motion by performing energy minimization at a series of fixed hinge angles allowing geometry optimization of all other structure parameters. This potential is shown in Fig. 6 and is reasonably harmonic. The approximate probability distribution of the hinge angle in the zero-point energy level, calculated in the harmonic limit, is

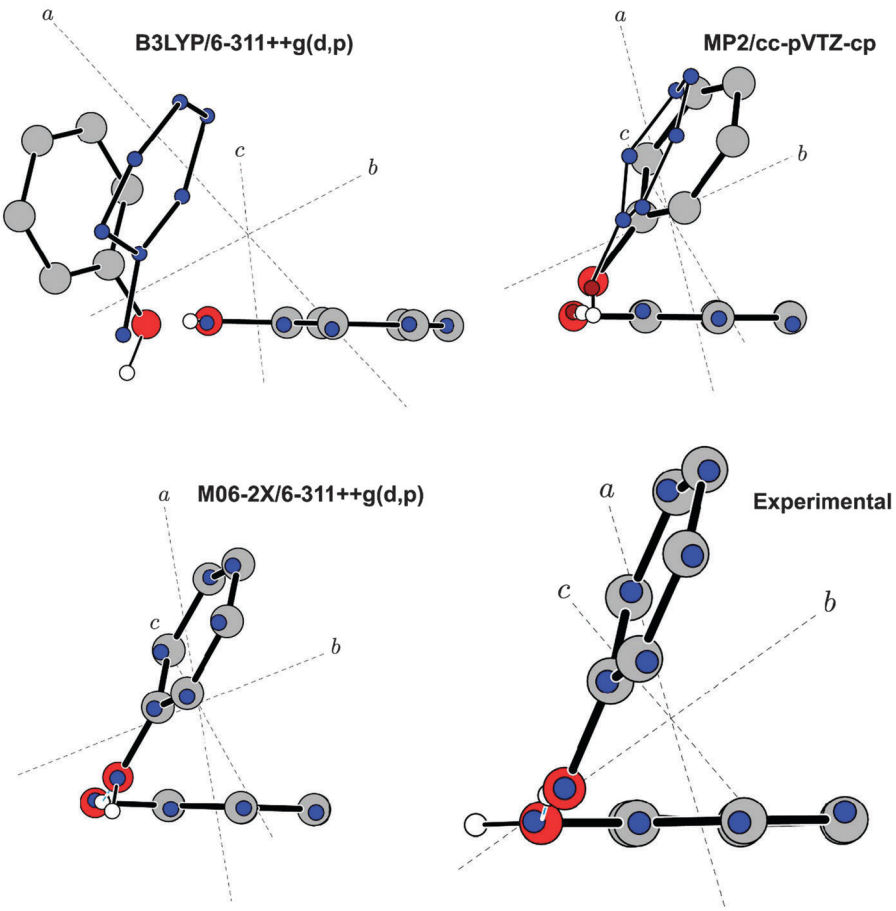

Fig. 5 Comparison of theoretical and an experimental structure of phenol dimer with the r_s (Kraitchman) results. The small blue circles represent the r_s coordinates, and the larger connected frameworks represent the labeled *ab initio* method used, except for the Experimental entry (which uses the r_0 structure as the framework).

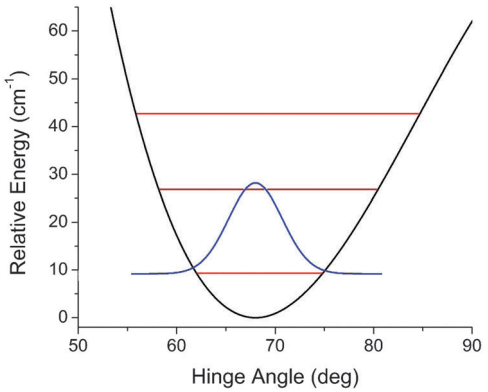

Fig. 6 Phenol dimer ''hinge'' potential energy surface, calculated at the M06-2X/6-311g(d,p) level of theory. The total *harmonic* probability distribution for the ground state (blue) suggests a hinge angle of 68.0(39)°. The ground state and the first two excited vibrational states (red) are shown at their calculated anharmonic frequencies.

shown in the figure. The calculated quantum mechanical fluctuation in the harmonic limit is about ±3.9° (1σ), which is smaller than the variation of hinge angles seen in the calculations tabulated in Table 3. The *ab initio* potential energy surface data was fit to a cubic function of the form $a\theta^3 + b\theta^2$ (a = −0.004472 cm^{-1}, b = 0.232 cm^{-1}, R^2 = 0.99). The cubic corrections were made using standard second order perturbation theory. The reduced mass for the normal mode associated with this hinge angle is 5.5868 amu, which leads to a harmonic force constant of 0.255 N m^{-1}. A full listing of the unscaled harmonic vibrational frequencies for phenol dimer can be found in the ESI.†

Finally, we have performed a refined r_0 structure determination using STRFIT[38] that combines the experimental isotopic data with some constraints from the M06-2X/6-311++g(d,p) theoretical structure. The bond lengths and angles within each phenol unit are fixed to their theoretical values (and these are essentially identical to the geometry of the phenol monomer). This constrains the heavy atoms in each phenol unit to be planar. The torsional angle of the –OH group for each phenol molecule is also constrained to the theoretical value. The hydroxyl hydrogen atom in each phenol is close to the plane of its heavy atoms (dihedral angles of 0.633° and 2.336° are calculated for the donor and acceptor rings, respectively). Therefore, the constraints from theory are close to assuming that the phenol monomer geometry is unchanged by complexation. The appropriate fitted structural parameters, therefore, are those that determine the intermolecular structure of the cluster. These include the hinge angle, the O···O distance, and the angles and dihedrals that define the angles between the two planes of the phenol rings. With the simple assumption of a static monomeric structure, the required number of degrees of freedom to fit a good structure is reduced to 8, which is small compared to the number of experimental structural parameters obtained in this study (45, or 3 rotational constants from the parent species and each of the 14 assigned isotopologues). Therefore, the fitted structure can be well-determined precisely, and in fact the precision of the r_0 fit presented here is limited by the RMS error generated by inaccuracies in the *ab initio* structure. A separate r_0 fit with *ab initio* constraints taken from a MP2/cc-pVTZ-cp benchmark structure[19] shows similar intermolecular parameters to that of the M06-2X-derived r_0 structure, albeit with poorer determination (since the MP2 geometry is more inaccurate with respect to experimental positions). The MP2-derived r_0 hinge angle, 56.5(37)°, is slightly smaller than the angle determined with the M06-2X geometry, 62.3(14)°, so there is some spread in the determination of this parameter. However, all other intermolecular parameters appear consistent between the two determinations. In addition, comparison of the monomer parameters between the M06-2X and MP2 reveals no significant difference (within the confidence interval for the r_0 determination) between the two levels of theory.

In general, the large amplitude anharmonic hinge motion does not significantly affect the ground state structural determination. Any significant zero-point vibrational deformation of the ground state structure should reveal itself in a discrepancy between the r_0 and r_s geometries, since the r_0 fit structure does not account for zero-point vibrational motion, whereas the r_s geometry accounts for some with an additive constant factor to the ground state moments of inertia.[35] Therefore, if a significant zero-point contribution to the ground state molecular structure exists, it should reveal itself in a direct comparison of the r_0 and r_s geometries. However, Fig. 5 (bottom right panel) reveals that the agreement between these two experimental geometries is excellent. This guarantees that there is no significant contribution to the ground state geometry from the anharmonic hinge potential. The refined phenol dimer structure is shown in Fig. 3 (left) and Fig. 5 (bottom right) and the fitted r_0 structural parameters are reported in Table 4. A full listing of intra- and intermolecular parameters for the phenol dimer can be found in the ESI.†

The results of this r_0 fit clear up a number of inconsistencies between previous experimental results and *ab initio* predictions. For instance, previous studies had assumed a hydrogen bonding distance of over 3 angstroms.[1,24] However, *ab initio* results suggest that the hydrogen bond is actually more water-dimer like, with an O···O distance of about 2.8 Å, a prediction consistent with the r_0 distance of 2.833(21) Å. Microwave measurements of the water dimer report an O···O distance of 2.98(1) Å.[39] Additionally, the previous results have overestimated the inter-ring effects, where a more pronounced C–H···π effect is visible between the hydrogens of the acceptor ring and the π system of the donor. A comparison of the new r_0 with previously published results[24] can be found in Fig. 7.

The structure of the phenol trimer

The experimental carbon atom structure of the trimer obtained from a Kraitchman analysis is shown in Fig. 3 where it is compared to the refined experimental structure obtained from constraining the M06-2X/6-311++g(d,p) *ab initio* structure. Because the parent species is a symmetric top, the Kraitchman analysis provides only two structure parameters for each ^{13}C atom: the coordinate of the atom on the symmetry axis and the distance of the atom from the symmetry axis. The relative angle

Table 4 Fitted r_0 intermolecular parameters for phenol dimer for two sets of *ab initio* constraints (M06-2X/6-311++g(d,p) and MP2/cc-PVTZ-cp), with comparisons to the M06-2X/6-311++g(d,p) *ab initio* structure used and a previous high resolution UV study.[24] The MP2/cc-pVTZ-cp values come from benchmark calculations found in ref. 19. Some parameters fitted in this study (such as C–O bond lengths) are omitted from this table; a full listing for the M06-2X and MP2-derived r_0 structures can be found in the ESI

Parameter	M06-2X/6-311++g(d,p)	MP2/cc-pVTZ-cp	r_0, M06-2X/6-311++g(d,p)	r_0, MP2/cc-pVTZ-cp	UV study, r_0
r(H···O)	1.889	1.873	1.837(23)	1.879(38)	2.354(49)
r(O···O)	2.833	2.833	2.833(21)	2.830(36)	3.221(25)
∠(O7–H7–O8)	168.05	170.50	170.5(21)	166.2(37)	150.6(18)
∠(C9–O8–H7)	118.88	122.48	122.5(10)	125.8(18)	138.6(15)
t(O8–H7–O7–C1)	85.07	128.97	75.5(59)	87(12)	109.6(45)
t(C9–O8–H7–O7)	−23.41	−41.22	−27.7(47)	−35(10)	−26.5(46)
t(C10–C9–O8–H7)	14.18	14.86	10.6(17)	14.8(44)	−1.0(19)
t(C1–O7–O8–C9) (hinge)	59.61	48.17	64.0(13)	56.5(37)	63.0[a]

[a] Value taken from r_s parameters reported in the UV study,[24] since no r_0 value was reported.

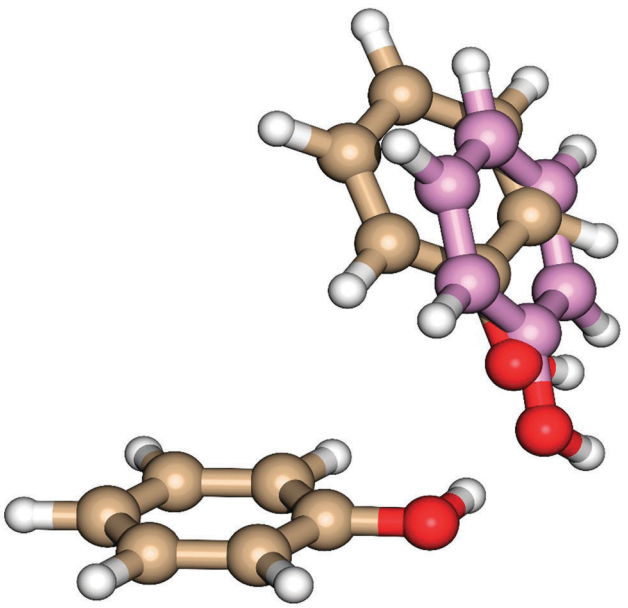

Fig. 7 Comparison of the new r_0 structure (purple) with the previously published r_0 structure by Schmitt *et al.* (brown). The donor rings of both structures are overlapping in order to emphasize the differences in the intermolecular geometry (''new'' donor ring not shown).

of rotation around the symmetry axis between two ^{13}C atoms was determined by requiring the distance of each carbon atom to the selected reference atom (the ^{13}C–O position) to equal the C–C distance in the phenol monomer (the theoretical structures show that the geometry of the phenyl group is essentially unchanged by complexation). These distance constraints determine the relative positions of the carbon atoms in a single phenyl ring, the other two positions are generated by (2π/3) rotations of the coordinate positions around the symmetry axis to generate the symmetric top structure.

Theoretical results are generally consistent across varying levels of theory, unlike phenol dimer. Use of diffuse functions in the Pople basis set appears to slightly improve predictions with respect to experiment, but not to the dramatic extent seen in the dimer. MP2 results agree well with the M06-2X/6-311++g(d,p) theoretical structure reported in this study. As with the dimer, the dispersion plays a crucial role in determining the complexation geometry, and use of B3LYP causes the barrel-like structure to open up into an *asymmetric* umbrella structure. These results, with comparison to the experimental rotational constants, can be found in Table 6.

A refined $r_m^{(1)}$ structure using constraints from the M06-2X/6-311++g(d,p) theoretical structure is shown in Fig. 3. Like the phenol dimer analysis, the constraints from theory fixed the geometry of each phenol rings where, also for the trimer, the calculated phenol geometry in the cluster is essentially the same as the phenol monomer. $r_m^{(1)}$ was chosen over r_0 due to the lack of experimental ^{18}O positions. Without these positions, r_0 determination of oxygen-containing structural parameters was poorer than $r_m^{(1)}$. This is due to the fact that the $r_m^{(1)}$ model functions very similarly to Kraitchman, except that the vibrational corrections, which are significant for atoms near the principal axes, are fit with three mass-dependent c_{ii} coefficients.[40] Kraitchman's equations, however, assume a constant mass-independent vibrational correction to the ground-state moments of inertia.[35] In the case of a symmetric top like phenol trimer, $c_{aa} = c_{bb}$, and c_{cc} cannot be determined due to the C_3 symmetry about the c-axis (in the prolate basis), so only one c_{ii} coefficient was fit. The fitted value for $c_{aa} = c_{bb}$, as well as the fitted intermolecular parameters for phenol trimer, can be found in Table 5. The experimental O···O distance is slightly shortened compared to phenol dimer, at 2.760(70) Å.

Table 5 Fitted $r_m^{(1)}$ intermolecular parameters for phenol trimer, with comparisons to the M06-2X/6-311++g(d,p). Due to the C_3 symmetry, these parameters are symmetric upon cyclic interchange of atoms A → A′ → A″ for all atoms A contained in the parameter

Parameter	M06-2X/6-311++g(d,p)	$r_m^{(1)}$
r(H···O)/Å	1.940	1.895(86)
r(O···O)	2.811	2.760(70)
r(C1–C1′)	4.010	3.967(83)
∠(O–O′–O″)/°	60.0	60.03(73)
∠(O–H···O′)	147.3	147.1(16)
∠(C1–O″···O′)	−23.4	−27.9(14)
∠(C1″–O″···O)	117.9	114.0(16)
∠(C1···C1′···C1″)	60.0	60.00(75)
t(C1–O–O′–C1′)	−6.42	−5.9(28)
t(O–O′–C1′–C6′)	85.2	85.2(33)
$c_{aa} = c_{bb}$/amu Å^2	—	1.140(85)

Table 6 Phenol trimer rotational constants in the oblate basis for various levels of theory, compared to experiment. The experimental *A* constant is assumed based on the value of *C* in the isotopologues (prolate basis), since it cannot be fit experimentally

	A (MHz)	*B* (MHz)	*C* (MHz)
M06-2X/6-311g(d,p)	199.494	292.600	—
M06-2X/6-311++g(d,p)	198.084	290.540	—
MP2/6-311g(d,p)	205.635	296.244	—
MP2/6-311++g(d,p)	211.380	300.117	—
B3LYP/6-311++g(d,p)	240.6	222.786	130.919
Experiment	[188]	282.280790(56)	

This is similar to observations of water trimer *versus* dimer, where the trimer O···O distance is shortened from 2.98 Å to 2.85 Å due to stabilizing three body effects.[41] Additionally, a C–H···π interaction is apparent, where the *ortho* hydrogen of a donor ring coordinates with the 5–6 bond in the acceptor ring. This creates a roughly perpendicular arrangement of the rings in the barrel (the dihedral O···O′–C1′–C6′ is 85.2(33)° in the $r_m^{(1)}$ structure). In this case, it appears that parallel π stacking is not optimal for stable complexation, as the rings try to associate in as perpendicular of a fashion without sacrificing the monomer planarity and hence the water trimer-like hydrogen bonding motif. The full set of $r_m^{(1)}$ coordinates, as well as *ab initio* and r_s coordinates, can be found in the ESI.†

A recent study by Yang and Waller on cooperative effects in gas-phase homotrimers reveals common threads between the results presented here for phenol trimer and the benchmark molecules used in their study, and sheds additional light on the efficacy of theoretical methods in treating the cooperative effects between dispersion and hydrogen bonding.[42] Yang and Waller note that use of a limited basis set in an RI-MP2 calculation can lead to significant differences when extrapolating to the complete basis set (CBS) limit in three-body interaction energies, sometimes up to 5% (for methanol trimer). However, as seen with our success with M06-2X, they note that dispersion-modified DFT calculations tend to give the best balance between computational cost and accuracy. Similar results were found for the interplay between hydrogen bonding and interring dispersion, where direct parallel π stacking is an inefficient complexation geometry for molecules that contain hydrogen bonding interactions.

Conclusion

In this study, we have determined the structures for phenol dimer and trimer through the use of chirped-pulse FTMW spectroscopy in the 2–8 GHz band. For the dimer, the r_s and least-squares fit r_0 geometries are improved over previously reported experimental geometries when compared to the best available theoretical structures. The dimeric structure is found to represent a case where an interplay between dispersion and hydrogen bonding play an essential role in fixing the complexation geometry, with a water dimer-like O···O distance of 2.833(21) Å, and a small dihedral between the rings of 62.3(14)°. However, both DFT and MP2 calculations struggle in determining an accurate structure. Instead, functionals like M06-2X and dispersion-modified DFT tend to give the most accurate results. For phenol trimer, a C_3 symmetric barrel-like helical structure is found, again with excellent agreement with the best available theoretical structures. The determined least-squares fit $r_m^{(1)}$ structure the three body interactions strengthen the hydrogen bonding in the trimer, with a shortened O···O distance of 2.760(70) Å, similar to that of water trimer.

With the new improvements to the 2–8 GHz CP-FTMW instrument design, structure determination of gas-phase clusters with over ten heavy atoms is becoming routine. In this regime of large gas-phase clusters, the complex interactions often involved in determining the actual global minimum cluster geometry is often a difficult problem for standard *ab initio* calculations to solve accurately and consistently. Therefore, it is important to supplement the theoretical methods with accurate experimental structures such as those for phenol dimer and trimer, in order to fine tune the accuracy of *ab initio* structures both for theory and for experimental predictions. Experimentally, this is especially important for large species with many isotopologues that are often weak in intensity and closely spaced together in a dense spectral region (like both species studied in this report), where a good theoretical geometry is required to make accurate scaled predictions for isotopologue rotational constants.

Acknowledgements

The authors acknowledge funding support from the National Science Foundation Major Research Instrumentation program (CHE-0960074). The authors also thank Zbigniew Kisiel for his always useful suggestions about structure determination.

References

1 P. Hobza, C. Riehn, A. Weicher and B. Brutschy, *Chem. Phys.*, 2002, **283**, 331.
2 R. Parthasarathi, V. Subramanian and N. Sathyamurthy, *J. Phys. Chem. A*, 2005, **109**, 843.
3 M. Kolář and P. Hobza, *J. Phys. Chem. A*, 2007, **111**, 5851.
4 K. Kitaura and K. Morokuma, *Int. J. Quantum Chem.*, 1976, **10**, 325.
5 X. Wu, M. C. Vargas, S. Nayak, V. Lotrich and G. Scoles, *J. Chem. Phys.*, 2001, **115**, 8748.
6 J. Klimeš and A. Michaelides, *J. Chem. Phys.*, 2012, **137**, 120901.
7 M. D. Stromsheim, N. Kumar, S. Coriani, E. Sagvolden, A. M. Teale and T. Helgaker, *J. Chem. Phys.*, 2011, **135**, 194109.
8 R. Peverati and D. G. Truhlar, arXiv:1212.0944 [phys.chem-ph], 2012.
9 L. A. Burns, A. Vásquez-Mayagoitia, B. G. Sumpter and C. D. Sherill, *J. Chem. Phys.*, 2011, **134**, 084107.
10 K. E. Riley, M. Pitoňak, P. Jurečka and P. Hobza, *Chem. Rev.*, 2010, **110**, 5023.
11 K. Müller-Dethlefs and P. Hobza, *Chem. Rev.*, 2000, **100**, 143.
12 K. E. Riley and P. Hobza, *WIREs Comput. Mol. Sci.*, 2011, **1**, 3.
13 W. Wang, O. Donini, C. M. Reyes and P. A. Kollman, *Annu. Rev. Biophys. Biomol. Struct.*, 2011, **30**, 211.

14 R. R. Knowles and E. N. Jacobson, *Proc. Natl. Acad. Sci. U. S. A.*, 2010, **107**, 20678.
15 W. Tang, S. Johnston, J. A. Iggo, N. G. Berry, M. Phelan, L. Lian, J. Bacsa and J. Xiao, *Angew. Chem. Int. Ed.*, 2013, **52**, 1668.
16 J.-M. Lehn, *Chem. Soc. Rev.*, 2007, **36**, 151.
17 K. Fuke and K. Kaya, *Chem. Phys. Lett.*, 1982, **91**, 311.
18 K. Fuke and K. Kaya, *Chem. Phys. Lett.*, 1983, **94**, 97.
19 P. Jurečka, J. Šponer, J. Černy and P. Hobza, *Phys. Chem. Chem. Phys.*, 2006, **8**, 1985.
20 P. M. Felker, *J. Chem. Phys.*, 1992, **96**, 7844.
21 A. Weicher, C. Reihn and B. Brutschy, *J. Phys. Chem. A*, 2001, **105**, 5679.
22 T. Ebata, T. Watanabe and N. Mikami, *J. Phys. Chem.*, 1995, **99**, 5761.
23 T. D. Vaden and J. M. Lisy, *J. Chem. Phys.*, 2006, **124**, 214315.
24 M. Schmitt, M. Böhm, C. Ratzer, D. Krügler, K. Kleinermanns, I. Kalkman, G. Berden and W. L. Meerts, *ChemPhysChem*, 2006, **7**, 1241.
25 R. Brause, M. Santa, M. Schmitt and K. Kleinermanns, *ChemPhysChem*, 2006, **8**, 1394.
26 G. G. Brown, B. C. Dian, K. O. Douglass, S. M. Geyer, S. T. Shipman and B. H. Pate, *Rev. Sci. Instrum.*, 2008, **79**, 053103.
27 J. L. Neill, S. T. Shipman, L. Alvarez-Valtierra, A. Lesarri, Z. Kisiel and B. H. Pate, *J. Mol. Spectrosc.*, 2011, **269**, 21.
28 A. L. Steber, J. L. Neill, D. P. Zaleski, B. H. Pate, A. Lesarri, R. G. Bird, V. Vaquero-Vara and D. W. Pratt, *Faraday Discuss.*, 2011, **150**, 227.
29 E. J. Campbell, *Rev. Sci. Instrum.*, 1993, **84**, 2166.
30 J. K. G. Watson, *Mol. Phys.*, 1968, **15**, 479.
31 Y. Zhao and D. G. Truhlar, *Theor. Chem. Acc.*, 2008, **120**, 215.
32 Y. Zhao and D. G. Truhlar, *Acc. Chem. Res.*, 2008, **41**, 157.
33 M. J. Frisch, G. W. Trucks, H. B. Schlegel, G. E. Scuseria, M. A. Robb, J. R. Cheeseman, G. Scalmani, V. Barone, B. Mennucci, G. A. Petersson, H. Nakatsuji, M. Caricato, X. Li, H. P. Hratchian, A. F. Izmaylov, J. Bloino, G. Zheng, J. L. Sonnenberg, M. Hada, M. Ehara, K. Toyota, R. Fukuda, J. Hasegawa, M. Ishida, T. Nakajima, Y. Honda, O. Kitao, H. Nakai, T. Vreven, J. A. Montgomery Jr., J. E. Peralta, F. Ogliaro, M. Bearpark, J. J. Heyd, E. Brothers, K. N. Kudin, V. N. Staroverov, R. Kobayashi, J. Normand, K. Raghavachari, A. Rendell, J. C. Burant, S. S. Iyengar, J. Tomasi, M. Cossi, N. Rega, J. M. Millam, M. Klene, J. E. Knox, J. B. Cross, V. Bakken, C. Adamo, J. Jaramillo, R. Gomperts, R. E. Stratmann, O. Yazyev, A. J. Austin, R. Cammi, C. Pomelli, J. W. Ochterski, R. L. Martin, K. Morokuma, V. G. Zakrzewski, G. A. Voth, P. Salvador, J. J. Dannenberg, S. Dapprich, A. D. Daniels, Ö. Farkas, J. B. Foresman, J. V. Ortiz, J. Cioslowski and D. J. Fox, *Gaussian 09, Revision A.1*, Gaussian, Inc., Wallingford, CT, 2009.
34 J. Kraitchman, *Am. J. Phys.*, 1953, **21**, 17.
35 C. C. Costain, *J. Chem. Phys.*, 1958, **29**, 864.
36 L. Rulísek, H. Valdés, V. Klusák, O. Exner, I. Stary and P. Hobza, *J. Comput. Chem.*, 2007, **29**, 861.
37 M. Schmitt, U. Henrichs, H. Müller and K. Kleinermanns, *J. Chem. Phys.*, 1995, **103**, 9918.
38 Z. Kisiel, *J. Mol. Spectrosc.*, 2003, **218**, 58.
39 T. R. Dyke and J. S. Muenter, *J. Chem. Phys.*, 1974, **60**, 2929.
40 J. K. G. Watson, A. Roytburg and W. Ulrich, *J. Mol. Spectrosc.*, 1999, **196**, 102.
41 F. N. Keutsch, J. D. Cruzan and R. J. Saykally, *Chem. Rev.*, 2003, **103**, 2533.
42 J. Yang and M. P. Waller, *J. Phys. Chem. A*, 2013, **117**, 174.